Theoretical Study of the pH-Dependent Photophysics Of N1,N^6-Ethenoadenine and N3,N^4-Ethenocytosine

Dan T. Major and Bilha Fischer*

Department of Chemistry, Gonda-Goldschmied Medical Research Center, Bar-Ilan University, Ramat-Gan 52900, Israel

Received: January 9, 2003; In Final Form: July 31, 2003

N1,N^6-ethenoadenine (N1,N^6-ϵA) and N3,N^4-ethenocytosine (N3,N^4-ϵC) nucleos(t)ides are widely used fluorescent biochemical probes. Interestingly, the fluorescence of these compounds is highly dependent on the acidity of the medium. It is well established that the neutral form of the N1,N^6-ϵA chromophore is responsible for its fluorescence, whereas the protonated form of N3,N^4-ϵC is slightly fluorescent. However, the origin of the pH-dependent fluorescence has remained elusive. In the current work, the electronic excitation and emission gas-phase spectra of 3-Me-N1,N^6-ϵA (**1**) and 1-Me-N3,N^4-ϵC (**2**) were calculated using configuration interaction singles (CIS), time dependent density functional theory, and multiconfigurational quasidegenerate second-order perturbation theory methods. The solvatochromic shift of **1** and **2** due to hydration was computed using a stepwise molecular dynamics-semiempirical CIS method. Good agreement between the computed and experimental spectra was obtained, both in the gas phase and in aqueous solution. Our results suggest that the pH-dependent loss of fluorescence of **1** is due to interaction between the lowest $\pi\pi^*$ and nπ^* excited states, which may lead to rapid radiationless decay to the ground state.

1. Introduction

The photophysical properties of the nucleic acid bases have been the subject of numerous experimental[1] and theoretical studies,[2] and it is well established that they are not significantly fluorescent.[3] However, several synthetic etheno(ϵ)-bridged bases, nucleosides, and nucleotides (Scheme 1) are fluorescent and are widely used in biochemical studies.[4] This is due to their structural similarity to the natural bases, yet very different photophysical behavior. Important applications of synthetic ϵ-nucleos(t)ides include their use as inhibitors,[5] allosteric effectors,[5] and coenzymes in enzymatic systems.[6] Additionally, the ϵ-bridged nucleos(t)ides are useful for the elucidation of the mode of action of chemical carcinogens such as vinyl chloride and ethyl carbamate or their metabolites.[7] Such carcinogens react with the bases of DNA and RNA to generate the cyclic ϵ-adducts, leading to base mismatching and subsequent mutation. Genetic stability is regained by specific enzymes, which remove the damaged base.[8−10]

A widely used synthetic ϵ-derivative is N1,N^6-ϵ-ATP (Scheme 1).[4,11] N1,N^6-Ethenoadenine nucleos(t)ides are highly fluorescent compounds with quantum yields of approximately 0.6, which permits their detection even at very low concentrations.[12] Upon excitation of N1,N^6-ϵA nucleos(t)ides at 300 nm, a fluorescence band with maximum at 410 nm is observed. Such long absorption and emission wavelengths allow selective excitation and detection respectively of the chromophore within a protein or nucleic acid environment. The fluorescent lifetime of N1,N^6-ϵA nucleos(t)ides is close to 20 ns, which enables detection of the chromophore with a variety of fluorescence spectroscopy methods. Recently, several derivatives of N1,N^6-ϵ-ATP were synthesized and proposed as fluorescent acidity probes of protein nucleotide binding sites.[13]

Closely related to the N1,N^6-ϵA nucleos(t)ides are the N3,N^4-ethenocytosine analogues (Scheme 1).[4,11] The emission spectra of N3,N^4-ϵ C nucleotides in aqueous solution reveal a maximum at 340 nm.[14] Fluorescence excitation spectra have shown that the band at 288 nm is responsible for the fluorescence. However, the fluorescence intensity of the N3,N^4-ϵC nucleos(t)ides is significantly lower than for the adenine counterpart with quantum yields less than 0.01. The fluorescence lifetime of 30 ps is also considerably shorter than for the N1,N^6-ϵA analogues. It has been postulated that the carbonyl group is responsible for the low quantum yield of the N3,N^4-ϵC chromophore, due to a low-lying nπ^* transition originating from the carbonyl group.[14]

Interestingly, the photophysical properties of both N1,N^6-ϵA and N3,N^4-ϵC are highly dependent on the pH of the solution. The absorption spectra of both N1,N^6-ϵA and N3,N^4-ϵC show great variation with the acidity of the medium. Moreover, it is well established that the neutral form (pH > 5.5) of the N1,N^6-ϵA chromophore (**1a**) is responsible for its intense fluorescence,[12] whereas only the protonated form (pH < 3) of N3,N^4-ϵC (**2b**) is fluorescent (Scheme 2).[14] However, a theoretical basis for the pH-dependent absorption and fluorescence spectra has been elusive.

Previously, ϵ-adenine has been studied in the gas phase at a semiempirical level of theory.[15] In this paper, we present high-level computations of the excitation and emission spectra of the neutral and protonated forms of 3-Me-N1,N^6-ϵA (**1**) and 1-Me-N3,N^4-ϵC (**2**) (Scheme 2). The computed spectra were compared to the available experimental data for related chromophores, and a good agreement between the experimental and theoretical values was obtained. Unique features of the pH-dependent photophysics of **1** and **2** were rationalized, and the pH-dependent loss of fluorescence of **1** was interpreted on the basis of low-lying nπ^* states.[16] The computations employed the configuration interaction singles (CIS) method, time de-

* To whom correspondence should be addressed. Phone: 972-3-5318303. Fax: 972-3-5351250. E-mail: bfischer@mail.biu.ac.il.

10.1021/jp0340515 CCC: $25.00
Published on Web 09/30/2003

SCHEME 1: Representative Nucleic Acid Base Etheno Analogues

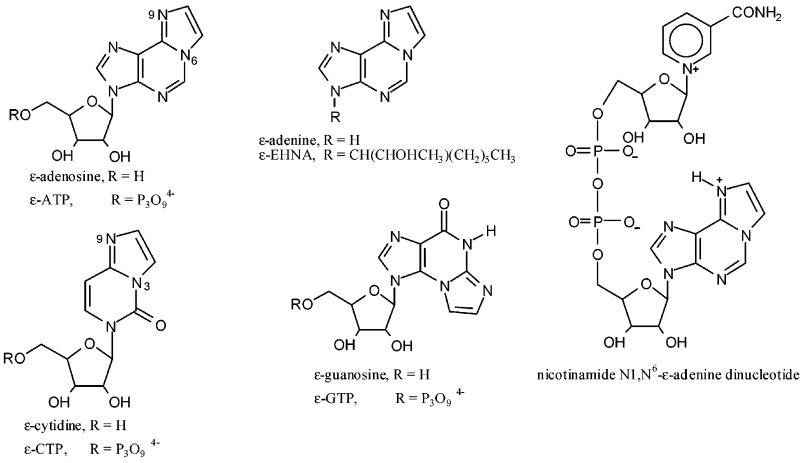

SCHEME 2: Neutral and Protonated 3-CH$_3$-N1,N^6-ϵA and 1-CH$_3$-N3,N^4-ϵC

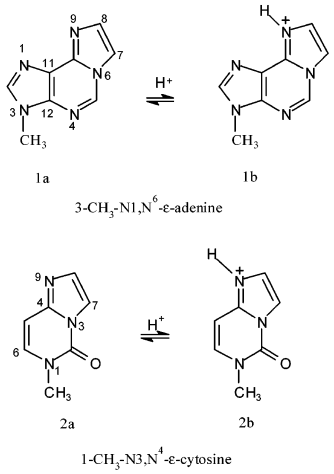

pendent density functional theory (TD-DFT) with pure and hybrid functionals, and multiconfigurational quasidegenerate second-order perturbation theory (MCQDPT2). The solvatochromic shifts due to hydration were treated using a discrete solvation approach combining molecular dynamics and semiempirical CIS quantum mechanics (MD-QM) in a stepwise manner. This combined classical mechanics-quantum mechanics approach was originally introduced by Coutinho and Canuto.[17]

2. Computational Methods

2.1. Ground and Excited-State Geometries. The ground-state geometries of **1a**, **1b**, **2a**, and **2b** (Scheme 2) were optimized using the B3LYP density functional[18] with the correlation consistent valence double-ζ cc-pVDZ basis set.[19] The optimizations used the Berny algorithm. The ground-state optimizations were performed using C_s symmetry. Frequency calculations were performed for all species to verify that the geometries found correspond to local minima on the geometry hypersurface.

Optimization of all excited states used the configuration interaction singles (CIS) method,[20] with the cc-pVDZ basis set. Excitation from all occupied orbitals was enabled through the FULL option. Excited-state optimizations were performed both in C_s and C_1 symmetry, and frequency calculations characterized the nature of the stationary points. If negative frequencies appeared, the geometry was reoptimized in the absence of symmetry, and the new stationary point was characterized. In the optimization of some excited states in C_1 symmetry, the nature of the excited state changed (state swapping), and the location of a local minimum was difficult. The problem was circumvented by adding the imaginary frequency normal modes from a prior frequency calculation of the excited state in C_s symmetry, as a perturbation to the state in C_1 symmetry.

2.2. Gas-Phase Electronic Transitions. Vertical electronic transitions were calculated using TD-DFT,[21] with the B3LYP and BPW91[22] functionals. The B3LYP functional has been shown to yield reliable excitation energies for low-lying states.[23] However, B3LYP and other hybrid functionals including exact exchange were recently shown to produce large errors for nπ* excitation energies.[24] Thus, we also employed the gradient corrected pure functional BPW91, which performs better for nπ* transitions. All TD-DFT calculations were performed in conjunction with the cc-pVDZ and aug-cc-pVDZ basis sets. The latter basis set is cc-pVDZ augmented with diffuse s, p, and d functions on heavy atoms and s and p functions on hydrogen atoms.

To supplement the TD-DFT results, ab initio MCQDPT2[25] calculations using the complete active space self-consistent field wave function as a reference were performed on the lowest $\pi\pi$* and nπ* transitions (excitation and emission). These calculations employed the 6-31G(d) basis set. The active space for each of the derivatives **1**−**4** were as follows: (**1**) 7 π, 3 lone-pair, and 3 π* orbitals yielding a total of 20 electrons in 13 orbitals (20, 13); (**2**) 7 π, 2 lone-pair, and 3 π* orbitals (18,12); (**3**) 6 π, 2 lone-pair, and 3 π* orbitals (16,11); (**4**) 6 π, 1 lone-pair, and 3 π* orbitals (14,10). In the calculation of excitation energies at the MCQDPT2 level, MP2/6-31G(d) geometries were employed.

2.3. Solvatochromic Shifts. The effect of aqueous solvation on the electronic spectra was investigated with a discrete solvent approach using a stepwise MD-QM method introduced by Coutinho and Canuto.[17] Initially, MD is used to generate a large number of configurations of the solute−solvent system. Subsequently, statistical analysis is performed on the MD trajectory data to extract a set of uncorrelated solute−solvent structures, which in general reduces the number of configurations by a factor of approximately 10^3. The radial distribution function is thereafter used to find the solvation shells surrounding the solute, enabling the effects of different solvation shells on the solute electronic structure to be investigated. The solute and the first few solvation shells are extracted from the MD trajectory and prepared for low-level quantum mechanical calculations. The set of uncorrelated solute−solvent configurations are then submitted to semiempirical CIS quantum mechanical calcula-

tions to obtain the solution phase electronic transitions, and these are compared to the gas-phase electronic transitions at the same level of theory. Finally, the solvatochromic shift is obtained as the average of the shifts of the uncorrelated structures.

The solvatochromic shifts of the absorption and emission bands of neutral and protonated 3-Me-N1,N^6-ϵA (**1a**, **1b**) and 1-Me-N3,N^4-ϵC (**2a**, **2b**) were investigated.

2.3.1. MD Simulations. Initially, MD simulations of the ground state and the lowest $\pi\pi^*$ excited state of **1a**, **1b**, **2a**, and **2b** were carried out in aqueous solution. The solute molecules were soaked in a previously equilibrated 31.1032^3 Å^3 cubic box of 1000 TIP3 water molecules. The water molecule O−H bonds were constrained using the SHAKE algorithm. The CHARMM 28b2 force field[26] was used and augmented with partial atomic charges for the solute atoms that were obtained from CHELPG[27] QM calculations. The charges for the ground-state molecules were obtained using the B3LYP/cc-pVDZ electron distribution, whereas the charges representing the relaxed excited $\pi\pi^*$ states were based on the CIS/cc-pVDZ electron distribution. The default CHARMM 28b2 vdW parameters were employed for all species. Test calculations on supermolecules of solute and individual water molecules showed that this is a reasonable approximation.[28] The solute molecules were kept frozen at their previously determined quantum mechanical geometry (B3LYP for ground states and CIS for excited states), eliminating the need to develop internal force field parameters (bond, angle, dihedral angle). Thus, solvent effects on the solute geometry were ignored. A theoretical study on adenine by Mennucci et al. has shown that this is not a serious concern.[2c] A cutoff of 13 Å was used for both electrostatics and vdW interactions in the MD simulations. Force switching and energy switching were used for electrostatic and vdW interactions, respectively.[29] The simulations were performed in the microcanonical (NVE) ensamble using the Leapfrog Verlet integration scheme. Periodic boundaries were used together with the minimum image convention. Initially the systems were heated from 0 to 300 K in the course of 5 ps followed by 10 ps of equilibration, and finally, the simulation was allowed to evolve for 200 ps.

The statistical inefficiency was calculated to obtain the correlation time for the simulation. For a discussion of the statistical details, the reader is referred to a work by Coutinho et al.[30] Briefly, the entire simulation is divided into n_b blocks of length t_b, and the total simulation length is given as $\tau = n_b t_b$. The statistical inefficiency, s,[31] was defined as

$$s = \lim_{t_b \to \infty} \frac{t_b \langle \delta E^2 \rangle_b}{\langle \delta E^2 \rangle} = \lim_{t_b \to \infty} S(t_b)$$

where $\langle \delta E^2 \rangle$ is the variance for the entire simulation, whereas $\langle \delta E^2 \rangle_b$ is the variance over blocks. The value of $S(t_b)$ increases with increasing t_b for correlated configurations until $S(t_b)$ reaches a limiting value, s, which is an estimate of the real correlation time. At the limiting value, the block size has reached a level where there is no correlation from block to block. Typically, in the present MD simulations the correlation time ranged from 1 to 2 ps.

The radial distribution functions were calculated to locate the boundaries of the solvation shells surrounding the solute. Three levels of systems were treated: solute and solvent including, (1) first, (2) first and half-second, and (3) second solvation shells. Uncorrelated solute−solvent configurations were extracted from the MD trajectory and prepared for the semiempirical QM calculations.

2.3.2. QM Calculations. The QM calculations of the solute and the water molecules within the relevant solvation shells were performed with the ZINDO method.[32] This involves a semiempirical CIS calculation with a window including the 10 highest occupied orbitals and the 10 lowest virtual orbitals. Typically, the final solvatochromic shift of an electronic transition, $\langle \Delta E \rangle$, was calculated as the average shift of approximately 100 uncorrelated configurations. To evaluate the influence of different solvation shells on the solvatochromic shift, $\langle \Delta E \rangle$ was computed at three levels of solvation: solute and the 1st, 1.5th, and 2nd solvation shells. Thus, for each molecule (**1a**, **1b**, **2a**, and **2b**) with a given geometry (ground and first excited $\pi\pi^*$ state), three ΔE values were obtained for each electronic transition. These three $\langle \Delta E \rangle$ values were plotted against the $1/r$ (reciprocal of the solvation shell distance). A linear regression analysis was performed and an estimation for $\lim_{r \to \infty} \langle \Delta E \rangle$ was obtained.

The statistical error due to the limited length of the simulation for a chain of uncorrelated configurations was defined as

$$\sigma(\langle \Delta E \rangle) = \sqrt{\frac{\langle \Delta E^2 \rangle - \langle \Delta E \rangle^2}{n - 1}}$$

where n is the number of uncorrelated configurations ($\approx$100), and $\langle \Delta E \rangle$ is the average solvatochromic shift.

All quantum mechanical CIS and TD-DFT calculations were performed using the Gaussian 98 package.[33] The MCQDPT2 calculations employed the GAMESS program.[34] Molecular mechanics calculations were performed using the CHARMM program.[35] All auxiliary programs used in the statistical and data analysis were written using the Perl 5.002 programming language. The calculations were performed on several SGI Origin 2000 computers at the Bar-Ilan University computer center and on an SGI O2 workstation in our laboratory.

3. Results and Discussion

3.1. Ground-State Structures. The structures of neutral and protonated 3-Me-N1,N^6-ϵA (**1a**, **1b**) and 1-Me-N3,N^4-ϵC (**2a**, **2b**) (Scheme 2) were optimized as described above and compared to the available experimental X-ray diffraction structures[36,37] (Table 1). Protonation of both N1,N^6-ϵA and N3,N^4-ϵC occurs at N9 as has been established by X-ray crystallography[36,37] and ^{1}H and ^{15}N NMR spectroscopy.[38,39]

Initially, the geometry of **1b** was optimized at several levels of theory to find the level most suited to describe the ground-state geometry. Both Hartree−Fock and B3LYP performed slightly better than MP2, and the inclusion of diffuse functions did not improve the agreement with experiment (results not shown). Thus we employed the B3LYP functional throughout for the ground-state geometries. The molecules were optimized both in C_s and C_1 symmetry, and in all cases, near-identical planar structures corresponding to local minima were obtained. Thus, the C_s symmetry optimized ground-state structures were used throughout to simplify the spectral assignments in the later stages. It is clear from Tables 1 and 2 that the geometries of **1b** and **2b** are satisfactorily described, with RMS errors of 0.019 Å and 0.017 Å for bond lengths and 1.2° and 0.82° for bond angles, respectively. The largest errors are found in the C11−C12 bridging double bond in 3-Me-N1,N^6-ϵA, as is reflected in both the bond lengths and angles of 3-Me-N1,N^6-ϵA. The absence of such a bridging bond in 1-Me-N3,N^4-ϵC is the main reason for the slightly better results for the ϵ-cytosine species.

The effect of protonation on the geometries of 3-Me-N1,N^6-ϵA and 1-Me-N3,N^4-ϵC may be seen by inspection of the results

TABLE 1: Ground State Structures of Neutral and Protonated 3-CH_3-N1,N^6-ϵA

	B3LYP/cc-pVDZ		X-ray[a]
cmpd.	**1a**	**1b**	**1b**
	Bond Distances (Å)		
N1−C2	1.320	1.321	1.311
C2−N3	1.375	1.379	1.368
N3−C12	1.381	1.369	1.399
N4−C12	1.357	1.350	1.360
N4−C5	1.305	1.301	1.291
C5−N6	1.377	1.390	1.380
N6−C10	1.423	1.382	1.379
C10−C11	1.425	1.400	1.413
C11−C12	1.402	1.411	1.362
N1−C11	1.375	1.367	1.384
N6−C7	1.390	1.404	1.415
C7−C8	1.375	1.359	1.346
C8−N9	1.376	1.389	1.397
N9−C10	1.319	1.349	1.329
N3−C1′	1.453	1.465	1.444
RMS deviation		0.019	
	Bond Angles (deg)		
N1−C2−N3	114.0	114.3	115.4
C2−N3−C12	105.5	105.8	104.3
N3−C12−C11	105.5	105.0	105.4
N4−C12−C11	128.4	127.2	128.6
C5−N4−C12	114.2	115.6	114.1
N4−C5−N6	123.4	122.7	123.0
C5−N6−C10	123.8	121.9	122.9
N6−C10−C11	113.6	117.6	115.4
C2−N1−C11	104.1	103.4	102.3
C10−C11−C12	116.5	114.9	115.9
N9−C10−C11	135.0	135.3	135.6
N1−C11−C12	110.8	111.6	112.5
C7−N6−C10	105.9	108.4	107.7
N6−C7−C8	105.2	106.9	106.0
C7−C8−N9	112.5	108.1	109.5
C8−N9−C10	105.1	109.5	107.9
C2−N3−C1′	128.2	127.5	126.1
RMS deviation		1.2	

[a] Reference 36.

TABLE 2: Ground State Structures of Neutral and Protonated 1-CH_3-N3,N^4-ϵC

	B3LYP/cc-pVDZ		X-ray[a]
cmpd.	**2a**	**2b**	**2b**
	Bond Distances (Å)		
N1−C2	1.393	1.398	1.376
C2−N3	1.402	1.425	1.404
N3−C4	1.399	1.366	1.353
C4−C5	1.429	1.412	1.393
C5−C6	1.356	1.368	1.348
C6−N1	1.391	1.370	1.381
N3−C7	1.386	1.395	1.395
C7−C8	1.375	1.359	1.326
C8−N9	1.380	1.392	1.378
C4−N9	1.320	1.348	1.333
C2−O10	1.218	1.204	1.208
N1−C1′	1.464	1.464	1.481
RMS deviation		0.018	
	Bond Angles (deg)		
N1−C2−N3	112.9	112.4	112.6
C2−N3−C4	126.2	124.7	124.8
N3−C4−C5	117.3	120.4	120.1
C4−C5−C6	117.8	115.7	117.1
C5−C6−N1	122.7	123.7	121.8
C6−N1−C2	123.2	123.1	123.6
C2−N3−C7	126.9	125.4	126.3
N3−C7−C8	104.8	106.3	106.8
C7−C8−N9	112.0	107.6	108.1
C8−N9−C4	105.1	109.9	109.5
N9−C4−C5	131.4	133.3	133.1
N1−C2−O10	124.6	126.2	125.7
C2−N1−C1′	117.7	117.3	118.0
RMS deviation		0.79	

[a] Reference 37.

in Tables 1 and 2. In 3-Me-N1,N^6-ϵA, the N9−C10 bond is elongated due to protonation reflecting an increased single bond character. Corresponding to this change is a shortening of the N6−C10 and C10−C11 bonds, reflecting the conjugation in the system. The largest changes in bond angles are found in the etheno ring as expected. Similarly to 3-Me-N1,N^6-ϵA, protonation of 1-Me-N3,N^4-ϵC leads to an increase in the C4−N9 bond length and a shortening in the C2−N3, N3−C4, and C4−C5 bond lengths. Likewise, the greatest changes in bond angles are confined to the etheno ring. The C−O distance is shortened, due to protonation, in agreement with infrared stretching frequency data.[14]

3.2. Gas-Phase Absorption Spectra. Initially, the performance of the ab initio MCQDPT2 method and the two density functionals chosen for this study was tested by comparing the computed excitation energies to the UV absorption spectrum of neutral 3-Me-N1,N^6-ϵA (**1a**) on PVA sheets.[40] To our knowledge, this is the only available experimental spectral data for isolated etheno derivatives. Four absorption bands were observed for 3-Me-N1,N^6-ϵA experimentally, and their values are recapitulated in Table 3 together with the computed bands. The two low energy bands were reported to have relatively weak extinction coefficients, whereas the two higher energy transitions exhibited significantly greater extinction coefficients (Table 3).[40] Comparison of the computed and experimental excitation energies in Table 3 reveals good agreement, especially at the MCQDPT2 and the TD-DFT B3LYP level. MCQDPT2 places the lowest $\pi\pi^*$ transition marginally below the experimental value, with an error of −0.02 eV. The errors in the computed excitation energies using the TD-DFT B3LYP functional are

TABLE 3: Vertical Excitation Energies,[a] ΔE^g_{abs} (eV), and Oscillator Strengths, *f*, of Neutral and Protonated 3-CH_3-N1,N^6-ϵA and 1-CH_3-N3,N^4-ϵC in the Gas Phase

		B3LYP[b]		BPW91[b]		MCQDPT2[c]	exp.[d]	
cmpd.	state	ΔE^g_{abs}	*f*	ΔE^g_{abs}	*f*	ΔE^g_{abs}	ΔE^g_{abs}	$\epsilon \times 10^{-3}$
1a	A′ ($\pi\pi^*$)	3.92	0.05	3.58	0.03	4.01	4.03	2.6
	A′ ($\pi\pi^*$)	4.68	0.00	4.39	0.01		4.51	6.0
	A′ ($\pi\pi^*$)	5.28	0.47	4.89	0.09		5.21	24.0
	A′ ($\pi\pi^*$)	5.39	0.16	5.08	0.40		5.58	15.0
	A″ ($n\pi^*$)	5.07	0.00	4.24	0.00	5.12		
	A″ ($n\pi^*$)	5.36	0.00	4.40	0.00			
1b	A′ ($\pi\pi^*$)	4.51	0.07	4.13	0.03	4.45		
	A′ ($\pi\pi^*$)	4.70	0.05	4.39	0.02			
	A′ ($\pi\pi^*$)	5.29	0.24	4.89	0.18			
	A′ ($\pi\pi^*$)	5.68	0.57	5.23	0.38			
	A″ ($n\pi^*$)	4.96	0.00	4.19	0.00	5.30		
	A″ ($n\pi^*$)	5.31	0.00	4.54	0.00			
2a	A′ ($\pi\pi^*$)	4.48	0.23	4.33	0.17	4.66		
	A′ ($\pi\pi^*$)	4.79	0.05	4.55	0.03			
	A′ ($\pi\pi^*$)	5.82	0.07	5.59	0.08			
	A′ ($\pi\pi^*$)	5.98	0.09	5.70	0.00			
	A″ ($n\pi^*$)	5.38	0.00	4.55	0.00	5.93		
	A″ ($n\pi^*$)	5.81	0.00	5.04	0.00			
2b	A′ ($\pi\pi^*$)	4.30	0.24	4.06	0.19	4.05		
	A′ ($\pi\pi^*$)	5.24	0.07	4.81	0.05			
	A′ ($\pi\pi^*$)	5.84	0.12	5.34	0.07			
	A′ ($\pi\pi^*$)	6.26	0.02	5.67	0.04			
	A″ ($n\pi^*$)	5.41	0.00	4.38	0.00	5.83		
	A″ ($n\pi^*$)	5.86	0.00	5.34	0.00			

[a] Only the four lowest $\pi\pi^*$ transitions and the lowest two $n\pi^*$ transition are shown. [b] The aug-cc-pVDZ basis set was used. [c] The 6-31G(d) basis set was used. [d] 3-CH_3-N1,N^6-ϵA on PVA sheets (ref 40).

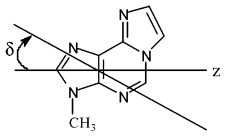

1a

Figure 1. Definition of the in-plane angle relative to the *z* axis of 3-CH$_3$-N1,N^6-ϵA.

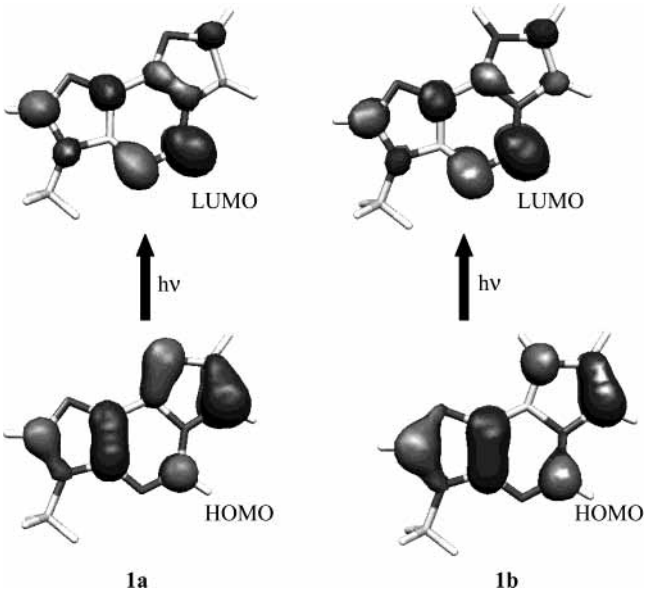

Figure 2. Molecular orbitals involved in the first $\pi\pi^*$ transition of neutral and protonated 3-CH$_3$-N1,N^6-ϵA.

(from red to blue) −0.11, 0.17, 0.07, and −0.19 eV. The BPW91 functional underestimates all four transitions with an average error of 0.35 eV. The computed B3LYP oscillator strengths (*f*) indicate that the two bands to the red should have relatively low intensity, whereas the two blue bands should be considerably more intense in agreement with the experiment. Unfortunately, no nπ^* transitions were observed in the experimental absorption spectrum, leaving the computed values uncontested. The BPW91 functional places the two nπ^* transitions in proximity of the second $\pi\pi^*$ transition, whereas TD-DFT B3LYP and MCQDPT2 both place the lowest nπ^* transition at a higher energy (Table 3).

The computed transition band polarizations of **1a** provide additional support for the assignment of the computed electronic transitions to the experimental bands. The calculated transition dipole moment directions for the four lowest $\pi\pi^*$ transitions were −149, +51, −29, and +139° at the B3LYP level compared to the experimental values of −154, −47, −30, and +131° (Figure 1). The only discrepancy is related to the second $\pi\pi^*$ transition. However, this is a very weak transition (Table 3), which possibly includes overlapping nπ^* transitions, and this could be the reason for the poor agreement.

The calculated gas-phase absorption spectrum for the N9 protonated 3-Me-N1,N^6-ϵA (**1b**) reveals similarity to that of the neutral species, with the exception of the first $\pi\pi^*$ transition which is shifted far to the blue, leaving the first two transitions overlapping (Table 3). This first transition is composed mainly of a HOMO → LUMO excitation (Figure 2), for both the neutral and charged species. Examination of partial atomic charges and the Kohn−Sham frontier orbitals of the neutral and charged molecules may add some insight to the pH-dependent shift. The Mülliken charges of **1a** and **1b** in the ground state indicate an increase in the positive charge at the N9 position due to

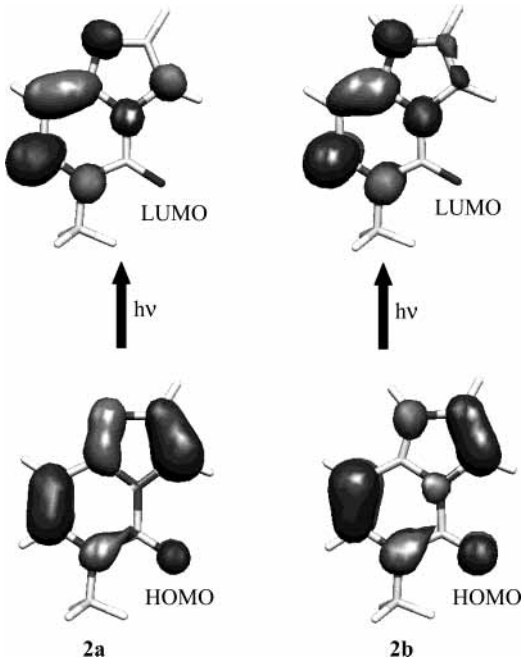

Figure 3. Molecular orbitals involved in the first $\pi\pi^*$ transition of neutral and protonated 1-CH$_3$-N3,N^4-ϵC.

protonation (−0.27 vs +0.13). Thus, a transition involving excitation from an orbital located also at the N9 position should be more demanding energetically in **1b** than in **1a**. Inspection of the HOMO → LUMO excitation in both **1a** and **1b** reveals a loss in electron density at the N9 position, the site of protonation in **1b** (Figure 3). Thus, there is an unfavorable removal of electron density from the already partially positively charged N9 atom that could explain why the first electronic transition is blue-shifted in the protonated species. Moreover, the HOMO → LUMO transition introduces antibonding character into the C10−C11 bond. This bond seems to be stronger in **1b** than in **1a** (Table 1), and therefore, the HOMO → LUMO transition should require more energy for the protonated species. In addition to affecting the transition energy quanta needed for the first excitation, protonation also increases the oscillator strengths of the four $\pi\pi^*$ transitions (Table 3). Although obtained in the gas phase, the pH-induced blue shift of the lowest $\pi\pi^*$ transition and the increase in band intensity well explain the experimental trend in the aqueous solution spectra of **1a** and **1b** (Table 4).[12]

The gas-phase spectrum of 1-Me-N3,N^4-ϵC (**2a**) exhibits four $\pi\pi^*$ transitions similarly to 3-Me-N1,N^6-ϵA (Table 3). However, in this case, the first $\pi\pi^*$ excitation (Figure 3) yields the largest oscillator strength, indicating that this transition should dominate the absorption spectrum. Protonation at the N9 position of 1-Me-N3,N^4-ϵC (**2b**) leads to considerable changes in the absorption spectrum. Most noticeable is the second band, which is shifted more than 0.5 eV to the blue at the B3LYP level. This transition is due mainly to excitation from HOMO to LUMO + 1 (Figure 4). It is interesting that the LUMO + 1 in 1-Me-N3,N^4-ϵC (**2a**) is fairly similar to the LUMO of the pyrimidine ring of 3-Me-N1,N^6-ϵA (Figure 2). In contrast to 3-Me-N1,N^6-ϵA, the oscillator strength of the two lowest $\pi\pi^*$ transitions are similar for the neutral and protonated species. Although obtained in the gas phase, the blue shift of the second $\pi\pi^*$ transition at low pH in conjunction with the similar band intensity seem to well explain the experimental trend in the aqueous solution spectra (Table 4).[14] An additional feature of the computed absorption spectrum of both neutral and protonated 1-Me-N3,N^4-ϵC is several low-lying nπ^* transitions, which are intercepted

TABLE 4: Solvatochromic Shifts, $\Delta\Delta E_{solv}$ (eV) and Vertical Excitation Energies,[a] ΔE^{s}_{abs} (eV) of Neutral and Protonated 3-CH_3-N1,N^6-ϵA and 1-CH_3-N3,N^4-ϵC in Aqueous Solution

		S-MD-QM	B3LYP[b]	BPW91[b]	MCQDPT2[c]	exp.	
cmpd.	state	$\Delta\Delta E_{solv}$	ΔE^{s}_{abs}	ΔE^{s}_{abs}	ΔE^{s}_{abs}	ΔE^{s}_{abs}	$\epsilon \times 10^{-3}$
1a	A′ ($\pi\pi^*$)	0.071 ± 0.004	3.99	3.65	4.08	4.13[d]	3.1
	A′ ($\pi\pi^*$)	−0.026 ± 0.002	4.66	4.36		4.51	6.0
						4.68	6.0
						≅4.81	5.0
	A″ ($n\pi^*$)	0.840 ± 0.016	5.91	5.08	5.96		
1b	A′ ($\pi\pi^*$)	0.103 ± 0.002	4.61	4.23	4.55	4.53[d]	11.0
	A′ ($\pi\pi^*$)	0.049 ± 0.003	4.75	4.43		4.68	10.0
	A″ ($n\pi^*$)	0.627 ± 0.004	5.58	4.82	5.93		
2a	A′ ($\pi\pi^*$)	0.063 ± 0.003	4.55	4.31	4.72	4.41[e]	11.1
	A′ ($\pi\pi^*$)	−0.068 ± 0.008	4.72	4.36		4.56	11.7
	A″ ($n\pi^*$)	0.273 ± 0.007	5.66	4.85	6.20		
2b	A′ ($\pi\pi^*$)	0.156 ± 0.002	4.46	4.22	4.21	4.31[e]	12.3
	A′ ($\pi\pi^*$)	−0.076 ± 0.006	5.16	4.74		5.00	4.4
	A″ ($n\pi^*$)	0.674 ± 0.018	6.09	5.06	6.50		

[a] Only the two lowest $\pi\pi^*$ transitions and the lowest $n\pi^*$ transition are shown. [b] The aug-cc-pVDZ basis set was used. [c] The 6-31G(d) basis set was used. [d] N1,N^6-ϵ-adenosine in aqueous solution (ref 41). [e] N3,N^4-ϵ-cytidine in aqueous solution (ref 14).

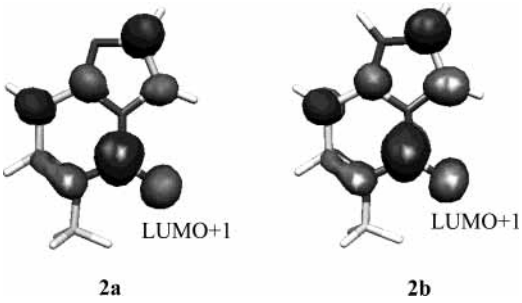

Figure 4. Virtual molecular orbitals involved in the second $\pi\pi^*$ transition of neutral and protonated 1-CH_3-N3,N^4-ϵC.

between the lowest lying $\pi\pi^*$ transitions. These excitations have their origin mainly in the carbonyl oxygen.

Several low-lying $\pi\sigma^*$ Rydberg states were observed for **1** and **2** using B3LYP/aug-cc-pVDZ. The σ^* orbitals were mainly antibonding with respect to C−H bonds.

3.3. Aqueous Solution Phase Absorption Spectra. The effect of aqueous solution on the electronic excitation spectra of **1** and **2** was investigated by the stepwise MD-QM method described above. A typical configuration of **1a** and the first two solvation shells is presented in Figure 5. In Table 4, the gas-phase spectra are combined with the solvatochromic shifts extrapolated to infinite solvation to give the computed absorption spectrum in aqueous solution.

Initially, it was of interest to evaluate the ability of the stepwise MD-QM method to reproduce the solvatochromic shift for 3-Me-N1,N^6-ϵA. Excitation energies were reported for 3-Me-N1,N^6-ϵA on PVA sheets[40] and for the related ϵ-adenosine in a nonpolar solvent (dioxane) and in aqueous solution.[41] Secrist et al. demonstrated that the longest wavelength band in N1,N^6-ϵ-adenosine exhibits a blue shift of 0.13 eV in aqueous solution relative to dioxane.[41] Additionally, the second main transition seems to show a slight red shift, although the interpretation of the second band is difficult. The computed solvatochromic shift of the first $\pi\pi^*$ transition of 3-Me-N1,N^6-ϵA in water is 0.03 eV to the blue when accounting for the first solvation shell. Including half the second solvation shell increases the shift to 0.04 eV, whereas including the entire second solvation shell increases the shift to 0.05 eV (Figure 5). If the computed value is linearly extrapolated to $r = \infty$, a blue shift of 0.07 eV is obtained, narrowing the gap between the experimental and computational values (Table 4, Figure 6). This result emphasizes

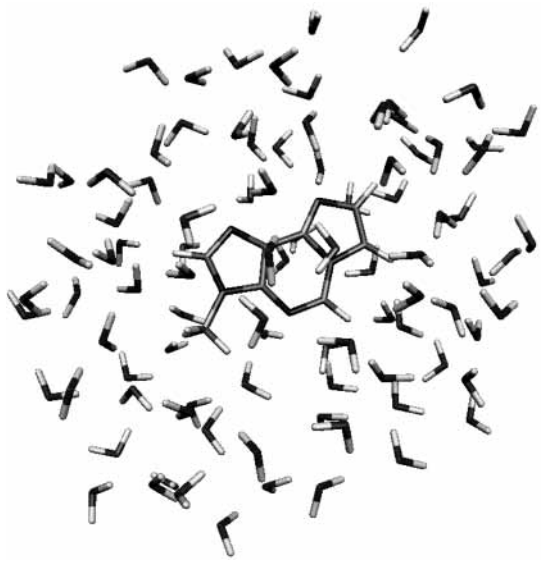

Figure 5. Sample configuration of 3-CH_3-N1,N^6-ϵA and the first two solvation shells.

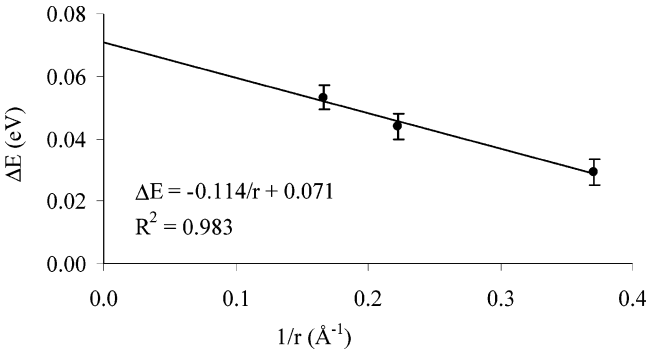

Figure 6. Solvatochromic shift (ΔE) of the lowest $\pi\pi^*$ state of 3-CH_3-N1,N^6-ϵA as a function of the solvation shell size ($1/r$).

the importance of long-range interactions on the computed spectra. For the second $\pi\pi^*$ transition of 3-Me-N1,N^6-ϵA, a slight red shift of 0.03 eV is predicted (Table 4). For both $\pi\pi^*$ transitions, addition of the solvatochromic shift to the gas-phase spectrum improves the agreement with the solution phase spectrum. The lowest $n\pi^*$ transition is shifted to the blue by 0.84 eV, in qualitative agreement with the expected shift due

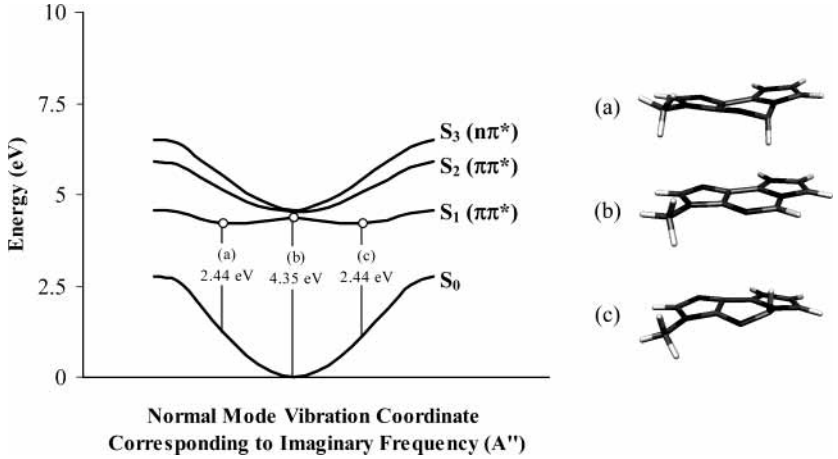

Figure 7. Gas-phase potential energy surface along the normal mode vibration coordinate corresponding to the imaginary frequency of the lowest $\pi\pi$* state (S_1) of protonated 3-CH_3-N1,N^6-ϵA at TD B3LYP/Aug-cc-pVDZ//CIS/6-31G level. Structure (b) corresponds to the local maximum on the S_1 surface, whereas (a) and (c) correspond to the local minima of S_1.

to hydrogen bonding between water molecules and the heterocyclic in-plane lone-pairs.[42] Considering the agreement between the theoretical and experimental solvatochromic shifts for **1a**, the combined MD-QM method is considered suitable for the current study.

The two lowest $\pi\pi$* transitions of protonated 3-Me-N1,N^6-ϵA (**1b**) are in good agreement with experiment. The best results are obtained at the MCQDPT2 level. Combining the energy of the lowest gas phase $\pi\pi$* transition with the solvatochromic shift yields an error of only 0.02 eV. Employing the B3LYP functional, the errors are only 0.06 eV for the first two bands. However, the error is even smaller before the solvent effect is added for this functional (Tables 3 and 4). Again, the solvent effects are much more pronounced for the nπ* transition, which is shifted far to the blue. The computed spectra of the ethenocytosine protomers (**2a** and **2b**) are also in good agreement with the experimental data.[14] The B3LYP computations place the two lowest $\pi\pi$* transitions of both neutral and protonated 1-Me-N3,N^4-ϵC at slightly higher energy than the experimental data. The errors are identical for **2a** and **2b**: 0.11 and 0.16 eV for the first and second transitions, respectively, using B3LYP (Table 4). The BPW91 functional also gives results in fair agreement with the experiment. It is noticeable that the MCQDPT2 results are not as accurate for the ϵ-cytosine species as for the ϵ-adenines, although the agreement is still good. In the work of Barrio et al.,[14] an additional shoulder was seen at the red edge of the spectra of **2a** and **2b** (4.25 and 4.11 eV, respectively). According to the current computational results, this is not a result of a weak $\pi\pi$* transition. Most likely this shoulder is due to a forbidden nπ* transition, originating from the carbonyl group or a $\pi\sigma$* transition.

3.4. Gas-Phase Emission Spectra. In the case of 3-Me-N1,N^6-ϵA (**1a**), the fluorescence at neutral pH is a result of excitation at 4.13 eV (300 nm) which corresponds to the lowest $\pi\pi$* state (Table 4).[12] The fluorescence of 1-Me-N3,N^4-ϵC in acidic solution (**2b**) originates from the second band at 4.31 eV (288 nm), as revealed by fluorescence excitation spectra.[14] According to our spectral assignments, this corresponds to the lowest $\pi\pi$* state (Tables 3 and 4). Thus, to obtain the relaxed fluorescent excited-state geometry, the first $\pi\pi$* excited states of 3-Me-N1,N^6-ϵA and 1-Me-N3,N^4-ϵC were optimized. The computed gas-phase emission energy of 3-Me-N1,N^6-ϵA (**1a**) is in fair agreement with the available experimental data,[40] with an error of 0.22 eV at the B3LYP level. Using the BPW91 functional, the error is marginal being only 0.03 eV. At the correlated ab initio level, the emission energy is overestimated by almost 0.5 eV, possibly due to the use of an uncorrelated CIS geometry for the excited molecule. The significant Stokes shift observed (0.59 eV at the B3LYP level) is due to relaxation of the excited $\pi\pi$* state geometry. For protonated 3-Me-N1,N^6-ϵA, a large Stokes shift of 2.07 eV is observed. This is due to the out-of-plane distortion of the excited $\pi\pi$* state geometry. This state possesses a double minima potential energy surface with the nonplanar structures (a) and (c) corresponding to local minima, whereas the C_s symmetrical structure (b) corresponds to a local maximum (Figure 7). The emission bands of neutral and protonated 1-Me-N3,N^4-ϵC exhibit significant Stokes shifts, especially at the TD-DFT levels. This is due to vibrational relaxation of the excited states, as is the case for the ϵ-adenine species.

3.5. Solution Phase Emission Spectra. The effect of hydration on the emission spectra of **1** and **2** was investigated by the stepwise MD-QM method described above. In Table 6, the gas-phase transitions are combined with the solvatochromic shifts to give the aqueous phase emission spectra.

The quality of the results may be assessed by comparing the solvatochromic shift of **1a** with the available experimental data. The fluorescence band of N1,N^6-ϵ-adenosine exhibits a red shift of 0.03 eV in aqueous solution relative to dioxane. The computed solvatochromic shift of 3-Me-N1,N^6-ϵA is -0.02 eV in good agreement with the experimental data. Thus, the MD-QM approach adequately describes the solvent effect on the excited states.

Although N9-protonated 3-Me-N1,N^6-ϵA (**1b**) is not fluorescent, a very weak fluorescence band with a 1 ns lifetime was observed at 2.79 eV for ϵ-adenine in acidic solution.[43] Combining the gas-phase emission energy and the solvatochromic shift, the computed emission energy of protonated 3-Me-N1,N^6-ϵA is 2.70 eV at the B3LYP level, and this seems to match the experimental data.

The computed maximum emission energy of protonated 1-Me-N3,N^4-ϵC is 0.4 eV above the experimental value of 3.70 eV using B3LYP, whereas using BPW91, the error drops to 0.23 eV. The MCQDPT2 level of theory overestimates the emission energy by 0.32 eV.

4. Discussion

Several intriguing questions regarding the N1,N^6-ϵA and N3,N^4-ϵC nucleos(t)ides are posed by their complex photophysics. Specifically: (1) Why is the fluorescence of the N1,N^6-

TABLE 5: Vertical Emission Energies,[a] ΔE^{g}_{ems} (eV), and Oscillator Strengths, *f*, of Neutral and Protonated 3-CH_3-N1,N^6-ϵA and 1-CH_3-N3,N^4-ϵC in the Gas Phase

		B3LYP[b]		BPW91[b]		MCQDPT2[c]	exp.	
cmpd.	state	ΔE^{g}_{ems}	*f*	ΔE^{g}_{ems}	*f*	ΔE^{g}_{ems}	ΔE^{g}_{ems}	Φ (%)[d]
1a	A′ (ππ*)	3.33	0.04	3.08	0.03	3.60	3.11[e]	0.51
							3.06[f]	0.50
							3.02[g]	0.45
	A″ (nπ*)	4.68	0.00	3.78	0.00	5.50		
1b[h]	A′ (ππ*)	4.28	0.08	4.05	0.14	4.40		
		(2.44)	(0.04)	(2.24)	(0.03)	(2.87)		
	A″ (nπ*)	4.61	0.00	3.97	0.00	4.44		
2a	A′ (ππ*)	4.07	0.28	3.92	0.24	4.57		
	A″ (nπ*)	5.11	0.00	4.34	0.00	5.56		
2b	A′ (ππ*)	3.99	0.26	3.82	0.21	3.89		
	A″ (nπ*)	5.20		4.21	0.00	5.86		

[a] Only the lowest ππ* and nπ* transitions shown. [b] The aug-cc-pVDZ basis set was used. [c] The 6-31G(d) basis set was used. [d] Quantum yield. [e] 3-propyl-N1,N^6-ϵA in dioxane (ref 12). [f] N1,N^6-ϵA in DMF (ref 12). [g] N1,N^6-ϵ-adenosine in dioxane (ref 41). [h] The lowest excited state has C_1 symmetry (shown in parentheses).

TABLE 6: Solvatochromic Shifts, $\Delta\Delta E_{solv}$ (eV), and Vertical Emission Energies,[a] ΔE^{s}_{ems} (eV), of Neutral and Protonated 3-CH_3-N1,N^6-ϵA and 1-CH_3-N3,N^4-ϵC in Aqueous Solution

		S-MD-QM	B3LYP[b]	BPW91[b]	MCQDPT2[c]	exp.	
cmpd.	state	$\Delta\Delta E_{solv}$	ΔE^{s}_{ems}	ΔE^{s}_{ems}	ΔE^{s}_{ems}	ΔE^{s}_{ems}	Φ (%)[d]
1a	A′ (ππ*)	−0.021 ± 0.004	3.31	3.06	3.58	2.99[e]	0.56
	A″ (nπ*)	0.672 ± 0.013	5.35	4.45	6.17		
1b[h]	A	0.230 ± 0.003	2.70	2.47	3.10	≅2.79[f]	0.02
2a	A′ (ππ*)	0.047 ± 0.003	4.11	3.97	4.62		–[i]
	A″ (nπ*)	0.190 ± 0.010	5.30	4.53	5.75		
2b	A′ (ππ*)	0.126 ± 0.002	4.12	3.94	4.02	3.70[g]	< 0.01
	A″ (nπ*)	0.344 ± 0.008	5.54	4.56	6.20		

[a] Only the lowest ππ* and nπ* transitions are shown. [b] The aug-cc-pVDZ basis set was used. [c] The 6-31G(d) basis set was used. [d] Quantum yield. [e] N1,N^6-ϵ-adenosine in neutral aqueous solution, pH = 7 (ref 12). [f] N1,N^6-ϵA in acidic aqueous solution (ref 43). [g] N3,N^4-ϵ-cytidine in acidic aqueous solution (ref 14). [h] The lowest excited state has C_1 symmetry. [i] Negligible fluorescence.

ϵA nucleos(t)ides quenched at low pH? (2) Why is the N3,N^4-ϵC chromophore so much less fluorescent than the adenine counterpart?

It would be natural to approach the first question with protonation equilibria of analogues **1** in mind (Scheme 2). However, it has been demonstrated that the pH-dependent fluorescence is *not* a result of a change in the excited-state protonation equilibrium.[12,14] This is apparent from inspection of the ground and excited-state pK_a values of the N1,N^6-ϵA chromophore. A wide range of excited-state pK_a values have been suggested for N1,N^6-ϵ-adenosine: +4.0,[12] +1.10,[44] and −2.59.[45] Based on the accumulated data, Leonard suggested a pK_a of ca. 2 for the excited state,[4] which is below the ground-state pK_a value of 3.9. Thus, following excitation of the N1,N^6-ϵA chromophore at neutral pH, excited-state protonation is unlikely, implying that the observed fluorescence is that of the neutral species. The assumption that the neutral species is responsible for the fluorescence received additional support from the similar fluorescence spectra of ϵ-adenosine in aqueous solution (where protonation could occur) and that of 3-propyl-N1,N^6-ϵA in anhydrous dioxane (where protonation is impossible).[43] Moreover, the N9-methylated ϵ-nucleobase also exhibits diminished fluorescence, similar to that of the N9-protonated N1,N^6-ϵA chromophore.[43]

The loss of fluorescence in **1** due to protonation may be interpreted based on vibronic coupling between the absorbing ππ* state and a low-lying nπ* state. Such a ππ*−nπ* interaction may significantly lower the energy of the absorbing state and increase its overlap with the ground state.[16] Subsequently, rapid internal conversion may occur via an avoided crossing point or through a conical intersection.[46] Our computations for the neutral and protonated forms of 3-Me-N1,N^6-ϵA (**1a** and **1b**) may indicate that ππ*−nπ* vibronic coupling plays a role in the pH-dependent fluorescence of **1**. The optimized first excited ππ* state of **1b** displays a pseudo Jahn−Teller distortion with a double minimum with a distorted geometry of C_1 symmetry, whereas the symmetric C_s structure is a local maximum on the potential energy surface (Figure 7). The relaxed lowest excited state is of a mixed ππ*−nπ* character and is indicative of interaction between these states.[16] In clear contrast to the emerging picture for protonated 3-Me-N1,N^6-ϵA, the lowest excited state of the neutral species is a ππ* state of C_s symmetry, and there is a considerable energy gap between the lowest ππ* state and the nearest nπ* state. In this case, no vibronic mixing is expected between the lowest ππ* and nπ* states, and indeed this species is strongly fluorescent.

The N3,N^4-ϵC chromophore displays weak fluorescence (Φ < 0.01) at room temperature and acidic pH (**2b**), considerably lower than that of the N1,N^6-ϵA species. It has been postulated that the relatively low fluorescence of this molecule compared to that of **1a** is due to several low-lying nπ* states,[14] originating in excitation from the carbonyl oxygen lone-pairs to the LUMO. These low-lying nπ* states could facilitate internal conversion and thus serve as nonradiative sinks. However, our computations do not support this hypothesis. Although several low-lying nπ* states are seen at the TD-BPW91 level, this is not confirmed at the TD-B3LYP or MCQDPT2 levels of theory (Tables 5 and 6). Interestingly, a low-lying nπ* state originating in the carbonyl group was observed in a recent work on cytosine at the TD-B3LYP and CASSCF levels and found to be operative in ultrafast decay via a conical intersection.[47] Thus, the existence of a low-lying nπ* state should be detected at the TD-B3LYP level. Therefore, other mechanisms of deactivation are likely to be important in the ϵ-cytosine species. A possible explanation

for the low fluorescence of the ϵ-cytidine chromophore is the existence of several low-lying $\pi\sigma^*$ states that could be important in radiationless deactivation routes.[48]

5. Conclusion

The current work employed various computational approaches to rationalize the complex pH-dependent photophysics of the biochemically important N1,N^6-ϵA and N3,N^4-ϵC chromophores. The gas-phase excitation and emission spectra were calculated using the CIS, TD-DFT, and MCQDPT2 methods. Solvatochromic shifts were computed using a stepwise molecular dynamics and semiempirical CIS quantum mechanical approach. The computed excitation and emission spectra were in good agreement with the available experimental data, and this work should serve as an additional validation of the emerging TD-DFT method. This work suggests that the origin of the pH-dependent fluorescence of the 3-Me-N1,N^6-ϵA chromophore is the interaction between low-lying singlet $\pi\pi^*$ and nπ^* states, which may open a radiationless decay channel via an accessible conical intersection. Yet, we cannot rule out other deactivation processes such as intersystem crossing,[49] interplay of $\pi\sigma^*$ states,[48] or collisions with protons.[44]

Acknowledgment. This work was supported in part by the Marcus Center for Medicinal Chemistry. Dan T. Major thanks the Israeli Ministry of Science and Sports for financial support. The authors thank the Bar-Ilan University Computer Center for the generous supply of computing time.

Supporting Information Available: Z matrixes and graphs of solvation shifts vs solvation shell size for derivatives **1a**, **1b**, **2a**, and **2b**. This material is available free of charge via the Internet at http://pubs.acs.org.

References and Notes

(1) Nir, E.; Plutzer, Ch.; Kleinermanns, K.; de Vries, M. *Eur. Phys. J. D* **2002**, *20*, 317−329.

(2) (a) Fülscher, M. P.; Roos, B. O. *J. Am. Chem. Soc.* **1995**, *117*, 2089−2095. (b) Fülscher, M. P.; Serrano-Andrés, L.; Roos, B. O. *J. Am. Chem. Soc.* **1997**, *119*, 6168−6176. (c) Mennucci, B.; Toniolo, A.; Tomasi, J. *J. Phys. Chem. A* **2001**, *105*, 4749−4757.

(3) Callis, P. R. *Annu. Rev. Phys. Chem.* **1983**, *34*, 329−357.

(4) (a) Leonard, N. J. *CRC Crit. Rev. Biochem.* **1984**, *15*, 125−199. (b) Leonard, N. J. *Biochem. Mol. Biol.* **1992**, *3*, 273−297.

(5) (a) Secrist, J. A., III.; Barrio, J. R.; Leonard, N. J. *Science* **1972**, *175*, 646−647. (b) Caiolfa, V. R.; Gill, D.; Parola, A. H. *Biophys. Chem.* **1998**, *70*, 41−56.

(6) Barrio, J. R.; Secrist, J. A., III.; Leonard, N. J. *Proc. Natl. Acad. Sci. U.S.A.* **1972**, *69*, 2039−2042.

(7) (a) Bolt, H. M. *Crit. Rev. Toxicol.* **1988**, *18*, 299−309. (b) Park, K. K.; Surh, Y. J.; Steward, B. C.; Miller, J. A. *Biochem. Biophys. Res. Commun.* **1990**, *169*, 1094−1098.

(8) Hang, B.; Medina, M.; Fraenkel-Conrat, H.; Singer, B. *Proc. Natl. Acad. Sci. U.S.A.* **1998**, *95*, 13561−13566.

(9) Saparbaev, M.; Laval, J. *Proc. Natl. Acad. Sci. U.S.A.* **1998**, *95*, 8508−8513.

(10) Lau, A. Y.; Wyatt, M. D.; Glassner, B. J.; Samson, L. D.; Ellenberger, T. *Proc. Natl. Acad. Sci. U.S.A.* **2000**, *97*, 13573−13578.

(11) For historical reasons, we will name the bridging nitrogens in ethenoadenine N1 and N^6, although according to the numbering in Scheme 1 the labels N6 and N^9 would be correct. Likewise, in ethenocytosine, we will name the bridging nitrogens N3 and N^4 instead of N3 and N^9.

(12) Spencer, R. D.; Weber, G.; Tolman, G. L.; Barrio, J. R.; Leonard, N. J. *Eur. J. Biochem.* **1974**, *45*, 425−429.

(13) Fischer, B.; Kabha, E.; Gendron, F. P.; Beaudoin, A. R. *Nucleosides, Nucleotides Nucleic Acids* **2000**, *19*, 1033−1054.

(14) Barrio, J. R.; Sattsangi, P. D.; Gruber, B. A.; Dammann, L. G.; Leonard, N. J. *J. Am. Chem. Soc.* **1976**, *98*, 7408−7414.

(15) Evleth, E. M.; Lerner, D. A. *Photochem. Photobiol.* **1977**, *26*, 103−108.

(16) Lim, E. C. *J. Phys. Chem.* **1986**, *90*, 6770−6777.

(17) Coutinho, K.; Canuto, S. *Adv. Quantum Chem.* **1997**, *28*, 89−105.

(18) (a) Becke, A. D. *J. Chem. Phys.* **1993**, *98*, 5648−5652. (b) Lee, C.; Yang, W.; Parr, R. G. *Phys. Rev. B* **1988**, *37*, 785−789.

(19) (a) Dunning, T. H. *J. Chem. Phys.* **1989**, *90*, 1007−1023. (b) Kendall, R. A.; Dunning, T. H.; Harrison, R. J. *J. Chem. Phys.* **1992**, *96*, 6796−6806.

(20) Foresman, J. B.; Head-Gordon, M.; Pople, J. A.; Frisch, M. J. *J. Chem. Phys.* **1992**, *96*, 135−149.

(21) Stratmann, R. E.; Scuseria, G. E.; Frisch, M. J. *J. Chem. Phys.* **1998**, *109*, 8218−8224.

(22) (a) Becke, A. D. *Phys. Rev. A* **1988**, *38*, 3098−3100. (b) Perdew, J. P.; Wang, Y. *Phys. Rev. B* **1992**, 45, 13244−13249.

(23) Bauernschmitt, R.; Ahichs, R. *Chem. Phys. Lett.* **1996**, *256*, 454−464.

(24) Parac, M.; Grimme, S. *J. Phys. Chem. A* **2002**, *106*, 6844−6850.

(25) Nakano, H. *J. Chem. Phys.* **1993**, *99*, 7983−7992.

(26) (a) Foloppe, N.; Mackerell, A. D. *J. Comput. Chem.* **2000**, *21*, 86−104. (b) Mackerell, A. D. Banavali, N. K. *J. Comput. Chem.* **2000**, *21*, 105−120.

(27) Breneman, C. M.; Wiberg, K. B. *J. Comput. Chem.* **1990**, *11*, 361−373.

(28) We performed test calculations on supermolecules of solute and water molecules to assess the quality of the augmented CHARMM 28b2 force field. The minimum energy distances between **1a** and individual water molecules were computed at the HF level (ground state) and CIS level (excited state) and compared with interaction distances obtained using CHARMM with the ground and excited-state partial atomic charges. The average difference between the ab initio and CHARMM interaction distances was 0.01 Å. We found that this had a small effect on the electronic transitions (0.002 eV) and was similar for excitation and emission spectra.

(29) Steinbach, P. J.; Brooks, B. R. *J. Comput. Chem.* **1994**, *15*, 667−683.

(30) Coutinho, K.; de Oliveira, M. J.; Canuto, S. *Int. J. Quantum Chem.* **1998**, *66*, 249−253.

(31) Frenkel, D.; Smit, B. *Understanding Molecular Simulation. From Algorithms to Applications*; Academic Press: San Diego, CA, 1996; Appendix D, pp 381−384.

(32) Ridley, J.; Zerner, M. C. *Theor. Chim. Acta* **1973**, *32*, 111−134.

(33) Frisch, M. J.; Trucks, G. W.; Schlegel, H. B.; Scuseria, G. E.; Robb, M. A.; Cheeseman, J. R.; Zakrzewski, V. G.; Montgomery, J. A., Jr.; Stratmann, R. E.; Burant, J. C.; Dapprich, S.; Millam, J. M.; Daniels, A. D.; Kudin, K. N.; Strain, M. C.; Farkas, O.; Tomasi, J.; Barone, V.; Cossi, M.; Cammi, R.; Mennucci, B.; Pomelli, C.; Adamo, C.; Clifford, S.; Ochterski, J.; Petersson, G. A.; Ayala, P. Y.; Cui, Q.; Morokuma, K.; Malick, D. K.; Rabuck, A. D.; Raghavachari, K.; Foresman, J. B.; Cioslowski, J.; Ortiz, J. V.; Stefanov, B. B.; Liu, G.; Liashenko, A.; Piskorz, P.; Komaromi, I.; Gomperts, R.; Martin, R. L.; Fox, D. J.; Keith, T.; Al-Laham, M. A.; Peng, C. Y.; Nanayakkara, A.; Gonzalez, C.; Challacombe, M.; Gill, P. M. W.; Johnson, B. G.; Chen, W.; Wong, M. W.; Andres, J. L.; Head-Gordon, M.; Replogle, E. S.; Pople, J. A. *Gaussian 98*, revision A.7; Gaussian, Inc.: Pittsburgh, PA, 1998.

(34) Schmidt, M. W.; Baldridge, K. K.; Boatz, J. A.; Elbert, S. T.; Gordom, M. S.; Jensen, J. H.; Koseki, S.; Matsunaga, N.; Nguyen, K. A.; Su, S. J.; Windus, T. L.; Dupuis, M.; Montgomery, J. A. *J. Comput. Chem.* **1993**, *14*, 1347−1363.

(35) Brooks, B. R.; Bruccoleri, R. E.; Olafson, B. D.; States, D. J.; Swaminathan, S.; Karplus, M. *J. Comput. Chem.* **1983**, *4*, 187−217.

(36) Wang, A. H. J.; Dammann, L. G.; Barrio, J. R.; Paul, I. C. *J. Am. Chem. Soc.* **1974**, *96*, 1205−1213.

(37) Wang, A. H. J.; Barrio, J. R.; Paul, I. C. *J. Am. Chem. Soc.* **1976**, *98*, 7401−7408.

(38) Scheller, K. H.; Sigel, H. *J. Am. Chem. Soc.* **1983**, *105*, 3005−3014.

(39) Sharon, E.; Fischer, B. Unpublished results.

(40) Holmén, A.; Albinsson, B.; Nordén, B. *J. Phys. Chem.* **1994**, *98*, 13460−13469.

(41) Secrist, J. A., III.; Barrio, J. R.; Leonard, N. J.; Weber, G. *Biochemistry* **1972**, *11*, 3499−3506.

(42) Karelson, M.; Zerner, M. C. *J. Am. Chem. Soc.* **1990**, *112*, 9405−9406.

(43) Sattsangi, P. D.; Barrio, J. R.; Leonard, N. J. *J. Am. Chem. Soc.* **1980**, *102*, 770−774.

(44) Takahashi, S.; Nishimura, Y.; Tsuboi, M.; Kuramochi, T.; Inoue, Y. *J. Chem. Phys.* **1981**, *75*, 3831−3837.

(45) Vanderkooi, J. M.; Weiss, C. J.; Woodrow, G. V., III. *Biophys. J.* **1979**, *25*, 263−276.

(46) (a) Bernardi, F.; Olivucci, M.; Robb, M. A. *Chem. Soc. Rev.* **1996**, *25*, 321−328. (b) Applegate, B. E.; Barckholtz, T. A.; Miller, T. A. *Chem. Soc. Rev.* **2003**, *32*, 38−49.

(47) Ismail, N.; Blancafort, L.; Olivucci, M.; Kohler, B.; Robb, M. A. *J. Am. Chem. Soc.* **2002**, *124*, 6818−6819.

(48) Sobolewski, A. L.; Domcke, W.; Dedonder-Lardeux, C.; Jouvet, C. *Phys. Chem. Chem. Phys.* **2002**, *4*, 1093−1100.

(49) Agbaria, R. A.; Parola, H. P.; Gill, D. *J. Phys. Chem.* **1994**, *98*, 13280−13285.